

Scientific paper

# Synthesis, Crystal and Electronic Structure, and Thermal Behavior of a New Flame Retardant-Hardener [Cu(diethylenetriamine)<sub>2</sub>]Cl<sub>2</sub>·H<sub>2</sub>O for Epoxy Resins

Borys Mykhalichko<sup>1</sup>, Helen Lavrenyuk<sup>1</sup>, Volodymyr Olijnyk<sup>2</sup>, Yurii Slyvka<sup>3,\*</sup>, Oleg Mykhalichko<sup>4</sup> and Yuriy Starodub<sup>1</sup>

<sup>1</sup> Department of Physics and Chemistry of Combustion, Lviv State University of Life Safety, Lviv, UA-79007 Ukraine

<sup>2</sup> Faculty of Chemistry, University of Opole, Opole, PL-45052 Poland

<sup>3</sup> Department of Inorganic Chemistry, Ivan Franko National University of Lviv, Lviv, UA-79005 Ukraine

<sup>4</sup> Chemistry Laboratory, Limited Liability Company "FUCHS Oil Ukraine", Lviv, UA-79000 Ukraine

\* Corresponding author: E-mail: yurii.slyvka@lnu.edu.ua

Received: 11-09-2024

## Abstract

A copper(II) chelate complex with diethylenetriamine (*deta*), [Cu(*deta*)<sub>2</sub>]Cl<sub>2</sub>·H<sub>2</sub>O (**1**), was synthesized by direct interaction of solid copper(II) chloride dihydrate with *deta*. Complex **1** was characterized by X-ray structural analysis, infrared (IR) spectroscopy and differential scanning calorimetry (DSC) and was studied as a flame retardant-hardener for epoxy resins. The crystals of **1** consist of [Cu(*deta*)<sub>2</sub>]<sup>2+</sup> cations, Cl<sup>-</sup> anions and uncoordinated water molecules. Each Cu(II) atom is chelated with two tridentate molecules of *deta*, which bond to the central Cu(II) atom in a non-equivalent manner. This results in a distorted tetragonal bipyramidal environment around the Cu(II) atom. The crystal packing of the structural units in **1** is determined by both the dominant cation-anion interaction and strong hydrogen bonds, such as N–H...Cl, N–H...O, and O–H...Cl. Density functional theory (DFT) calculations were performed to determine the electron structure of **1** using the restricted formalism of B3LYP method with a 6-31G\* orbital basis set. The *d*-orbitals of the Cu<sup>2+</sup> ion are split due to the interaction of a tetragonal bipyramidal environment and the chelation, resulting in the visually observed dark blue color of crystals of **1**. This color closely corresponds to the calculated value of the visible light wavelength ( $\lambda = 661.37$  nm), which is related to the energy of photons absorbed by the complex ( $\Delta = 1.874$  eV).

**Keywords:** Copper(II) chelated complex, diethylenetriamine, synthesis, crystal and electronic structure, flame retardant-hardener.

## 1. Introduction

The study of complexation processes of *d*-metal salts, particularly inorganic salts of copper(I) and copper(II), with polydentate ligands such as polyamines, represents a significant area of research in modern chemistry.<sup>1</sup> These coordination compounds have been demonstrated to be highly effective catalysts and accurate models of active sites of copper-containing enzymes.<sup>2–9</sup> These are often used as the basis for new luminescent materials, and can be integrated into the polymer matrices of epoxy resins, effectively reducing their combustibility.<sup>10–16</sup> In addition, copper salts, especially chlorides, are widely used for the conversion of hydrocarbon

derivatives, and copper(I) and copper(II) salts have proven to be highly effective in preventing flame spread during the combustion of nitrogen-containing hydrocarbons such as polyamines.<sup>17–20</sup> The formation of Cu(II)←N coordination bonds and chelation of metal atoms by polyamine molecules make the interaction of copper(II) salts with polyamines an area of considerable scientific interest. In addition, the formation of copper(II) complexes plays an important role in achieving practical non-combustibility of organic ligands. These complexes inhibit the combustion of nitrogen-containing hydrocarbons due to the strong binding of polyamines by copper(II) salts. Consequently, inorganic copper(II) salts are highly effective flame retardants, particularly for

preventing the ignition of various polyamines, including epoxy resin hardeners. The factors that reduce the combustibility of polyamines were identified.<sup>21,22</sup> This opens up new avenues for the utilization of copper salts in the fabrication of polymeric materials based on epoxy-amine composites, which exhibit unparalleled resistance to combustion.<sup>23–26</sup>

The literature describes a wide range of polyamine complexes of copper(II) with a diverse crystal structure, many of which include Cu–N interaction.<sup>27–35</sup> Concurrently, nitrogen-containing polydentate ligands demonstrate an exceptional capacity to form chelate complexes in which the resulting heterocyclic fragments stabilize the structure. It would be of interest to investigate the interaction of inorganic copper(II) salts with polyamines, in particular polyethylenepolyamine (*pepa*), in order to study the stoichiometry and stereochemistry of the formed chelate complexes, with a special emphasis on the influence of the electronic structure of inorganic salts and the dentate nature of organic ligands. In addition, the ability of inorganic copper(II) salts to effectively inhibit the combustion of epoxy-amine composites should be discussed.

Chelate complexes such as  $[\text{Cu}(\text{deta})\text{H}_2\text{O}]\text{SO}_4 \cdot \text{H}_2\text{O}$ ,  $[\{\text{CuCO}_3(\text{deta})(\text{H}_2\text{O})\}_2] \cdot 6\text{H}_2\text{O}$ ,  $[\text{Cu}(\text{eda})(\text{deta})]\text{SiF}_6$ , and  $[\text{Cu}(\text{eda})_2(\text{H}_2\text{O})(\text{Cl})]\text{Cl}$  (where *eda* stands for ethylenediamine and *deta* for diethylenetriamine, both components of *pepa*) have been previously utilized as flame retardant-hardeners for epoxies.<sup>36–39</sup> These coordination compounds have the potential to significantly reduce the combustibility of epoxy-amine composites and improve their physicochemical and mechanical properties. Therefore, it would be beneficial to investigate the interaction of *deta* with copper(II) chloride and study the thermal behavior of the resulting coordination compound. This is because its crystalline phase can also be used as a flame retardant-hardener of epoxy resins.

The paper presents the synthesis of  $[\text{Cu}(\text{deta})_2]\text{Cl}_2 \cdot \text{H}_2\text{O}$  (**1**) crystals, along with X-ray crystal structure determination, infrared (IR) spectroscopy, differential scanning calorimetry (DSC), and density functional theory (DFT) calculations of its electronic and molecular structure. It should be noted that the unit cell dimensions of the crystals **1** at room temperature have already been determined,<sup>40</sup> but the crystal structure of this compound has not yet been studied.

## 2. Experimental

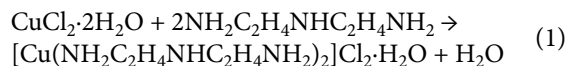
### 2.1. Materials

The chemicals  $\text{CuCl}_2 \cdot 2\text{H}_2\text{O}$  and diethylenetriamine (*deta*) were obtained from commercial sources and used as received without further purification.

### 2.2. Synthesis of $[\text{Cu}(\text{deta})_2]\text{Cl}_2 \cdot \text{H}_2\text{O}$

The crystals of bis(diethylenetriamine)copper(II) chloride monohydrate (**1**) were synthesized by direct in-

teraction of solid copper(II) chloride dihydrate with diethylenetriamine (*deta*). A homogeneous liquid mixture of dark blue color was obtained by triturating 1.70 g (10.0 mmol) of crystalline  $\text{CuCl}_2 \cdot 2\text{H}_2\text{O}$  in a porcelain mortar and adding 2.17 g (21.0 mmol) of *deta*. The contents were left at room temperature for several days until dark blue phase **1** crystals appeared as a reaction (1).



The product yield was 3.52 g (98%). Anal. calcd. (%) for  $\text{C}_8\text{H}_{28}\text{Cl}_2\text{CuN}_6\text{O}$ : C, 26.78; H, 7.87; N, 23.42; found: C, 26.57; H, 7.43; N, 23.54.

### 2.3. X-ray Crystal Structure Determination

Crystal **1** was mounted on an Xcalibur diffractometer equipped with an Oxford Cryosystem cooler and a CCD detector using  $\text{Mo } K_\alpha$  radiation (0.71073 Å) and a graphite monochromator. The diffraction data collected were processed using the CrysAlis PRO program.<sup>41</sup> The structure was solved using the ShelXT program and refined by the least-squares method in  $F^2$  using the ShelXL program with the graphical user interface OLEX2.<sup>42–44</sup> Atomic displacements for non-hydrogen atoms were refined using an anisotropic model. The ligand's amino groups' hydrogen atoms were obtained from Fourier difference syntheses and refined freely using isotropic displacement parameters. The remaining hydrogen atoms were placed at geometrically calculated positions and refined as riding atoms with relative isotropic displacement parameters. The crystal parameters, data collection, and refinement details are summarized in Table 1. All crystal structure figures were generated using the DIAMOND program.<sup>45</sup> Figure 1 displays the atom numbering system for the asymmetric part of complex **1**.

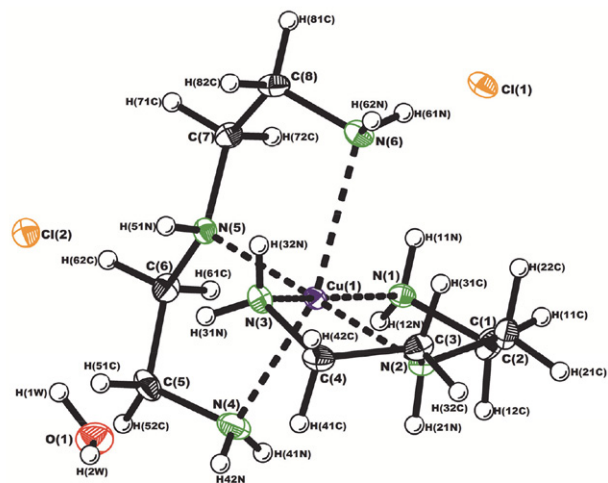


**Figure 1.** The atom numbering system for the asymmetric part of complex **1**. Thermal ellipsoids are shown at the 50% probability level for non-hydrogen atoms.

Table 1. Crystallographic and refinement data for **1**.

Empirical formula	C <sub>8</sub> H <sub>28</sub> Cl <sub>2</sub> CuN <sub>6</sub> O
$M_r$	358.80
Crystal system, space group	Monoclinic, $P2_1/c$
Temperature (K)	100(2)
$a, b, c$ (Å)	13.5036(2), 8.6387(1), 13.8853(2)
$\beta$ (°)	102.184(2)
$V$ (Å <sup>3</sup> )	1583.28(4)
$Z$	4
Radiation type	Mo $K_\alpha$
$\mu$ (mm <sup>-1</sup> )	1.717
$F(000)$	756
Measured reflections	1231
Independent reflections	4035
Observed reflections ( $I > 2\sigma(I)$ )	3591
$R_{int}, R_s$	0.0166, 0.0167
Refined parameters	206
$RI, wR2 [F^2 > 2\sigma(F^2)]$	0.0189, 0.0539
$RI, wR2$ [all data]	0.0225, 0.0550
Goodness of fit on $F^2$	1.039
$\Delta\rho_{max}, \Delta\rho_{min}$ (e <sup>-</sup> · Å <sup>-3</sup> )	0.464, -0.362

## 2. 4. Infrared Spectroscopy

The IR spectra of *deta* and [Cu(*deta*)<sub>2</sub>]Cl<sub>2</sub>·H<sub>2</sub>O were recorded using PerkinElmer Spectrum Two FTIR and Philips PU 9800 FT infrared spectrometers, respectively. Both spectra were recorded in the frequency range of 4000–500 cm<sup>-1</sup> with a resolution of 2 cm<sup>-1</sup>. The IR measurements were performed using a solid phase sample of **1** compressed into a pellet with spectroscopically pure KBr or a liquid phase sample of *deta* using a KBr cuvette. The recorded IR spectra of *deta* and [Cu(*deta*)<sub>2</sub>]Cl<sub>2</sub>·H<sub>2</sub>O are presented in Fig. 2.

## 2. 5. Differential Scanning Calorimetry

Differential Scanning Calorimetry data were obtained using a DSC1 Mettler Toledo instrument. The solid phase **1** (5.67 mg) was heated from room temperature to 350 °C at a rate of 10 °C per minute in a nitrogen environment in alumina crucible.

## 2. 6. Flammability Tests

The flammability of the *deta* and [Cu(*deta*)<sub>2</sub>]Cl<sub>2</sub>·H<sub>2</sub>O samples was evaluated by determining their ignition ( $t_{ign}$ ) and self-ignition ( $t_{self-ign}$ ) temperatures using a TF apparatus according to ASTM D1929-16.<sup>46</sup> The solid phase sample was prepared by compressing 3 g of crystalline **1** into a cylindrical tablet. The liquid phase sample of *deta* (3 g) was placed in an alumina crucible. Three measurements were taken for each type of sample and the resulting values were averaged.

## 2. 7. Computational Details

### 2. 7. 1. DFT Studies

The DFT method was used to perform quantum-chemical modeling of chelating processes in the *deta* – CuCl<sub>2</sub>·H<sub>2</sub>O system. The HyperChem program version 8.0.6 was used with a 6-31G\* orbital basis set and the restricted formalism of the B3LYP method.<sup>47</sup> Discrete clusters [Cu(*deta*)<sub>2</sub>]Cl<sub>2</sub>·H<sub>2</sub>O and [Cu(H<sub>2</sub>O)<sub>2</sub>Cl<sub>2</sub>] were constructed using crystallographic data from **1** and CuCl<sub>2</sub>·2H<sub>2</sub>O.<sup>48</sup> A free molecule of *deta* was also included. The charge density distribution was calculated for the discrete clusters without optimizing the geometry of structural fragments, while the geometry of the *deta* molecule was optimized. The calculations were performed assuming that the clusters and *deta* molecules were isolated and in a vacuum.

### 2. 7. 2. Hirshfeld Surface Analysis and Fingerprint Plots

To visualize the intermolecular interactions in the crystals of **1**, Hirshfeld surface analysis was performed. The three-dimensional Hirshfeld surfaces (HSs) and two-dimensional fingerprint plots for **1** were generated using the *Crystal Explorer* program.<sup>49</sup>

## 3. Results and Discussion

### 3. 1. Crystal Structure of [Cu(*deta*)<sub>2</sub>]Cl<sub>2</sub>·H<sub>2</sub>O

It is well known that nitrogen-containing tridentate ligands, such as *deta*, can form chelate complexes with copper(II) salts, including copper(II) halides. In these complexes, all three amino groups of the organic molecule coordinate with the central Cu(II) atom to form organometallic rings. The structure of these complexes, which have a general composition of CuX<sub>2</sub>·2*deta* (X = Cl, Br), is determined by the mode of coordination. Complex **1** is isostructural with previously studied complexes based on Co(II), Ni(II) and Zn(II) chlorides and with [Cu(*deta*)<sub>2</sub>]Br<sub>2</sub>·H<sub>2</sub>O complex.<sup>50–53</sup> In its crystal structure six N atoms from three amino groups of two *deta* molecules are coordinated to one copper(II) ion (Fig. 1 and Fig. 3) and the structure is composed of [Cu(*deta*)<sub>2</sub>]<sup>2+</sup> cations as the primary units and hydrated halide anions [Hal...HOH...Hal]<sup>2-</sup> as counterions.

The interaction of polyamines with copper(II) salts to form chelate complexes is reflected in the IR spectra in the form of a shift in the absorption bands for N–H bonds. Accordingly, our attention will be directed towards the absorption bands resulting from the stretching and bending of the –NH<sub>2</sub> and –NH– groups of the coordinated and free *deta* molecules. In the case of free *deta* (Fig. 2, a), the high-frequency region of 3366 and 3252 cm<sup>-1</sup> is associated with the stretching of

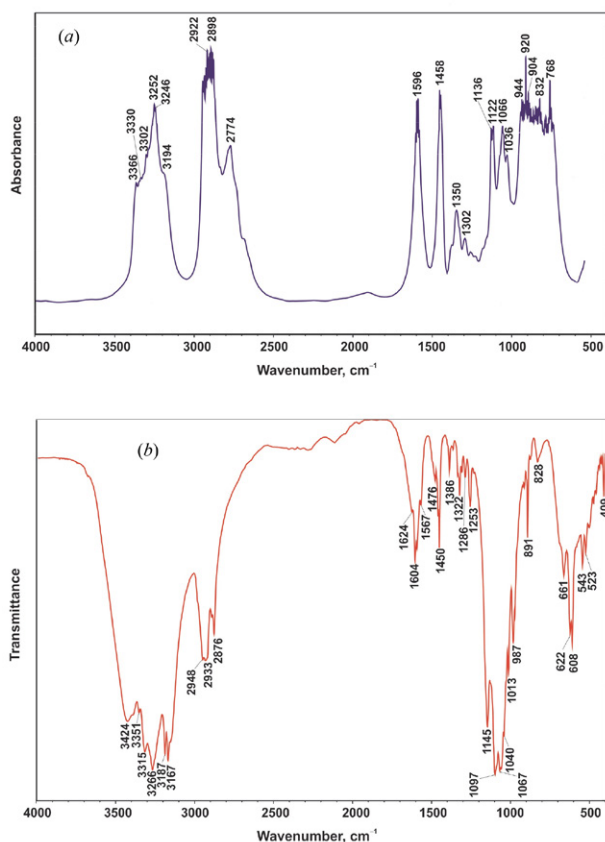


Figure 2. IR spectra of *deta* (a) and **1** (b).

N–H bonds in  $\text{-NH}_2$  groups. Furthermore, the band observed at  $3194\text{ cm}^{-1}$  is associated with the stretching of N–H bonds in  $\text{-NH-}$  groups. The vibration frequency at  $1596\text{ cm}^{-1}$  corresponds to the bending of N–H bonds. Following the bonding of the *deta* to  $\text{CuCl}_2$  (as illustrated in Fig. 2, b), two N–H absorption bands exhibited a shift in to a higher frequency, observed at  $3424$  and  $3266\text{ cm}^{-1}$ , while another band exhibited a shift in the opposite direc-

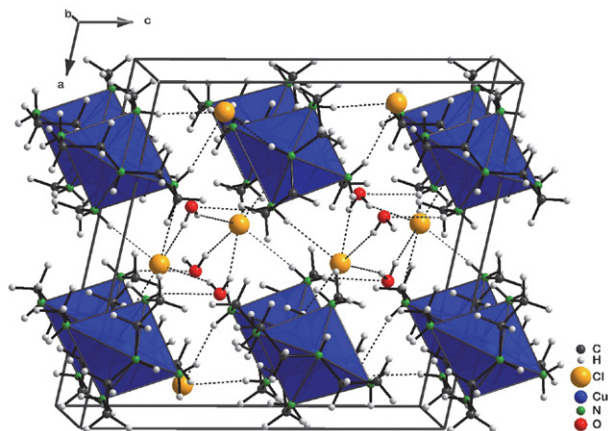


Figure 3. Crystal packing of **1** with presented tetragonal bipyramidal coordination of  $\text{Cu(II)}$ . Hydrogen bonds are shown as dotted lines.

tion, observed at  $3167\text{ cm}^{-1}$ . In addition, the wavenumber at  $1596\text{ cm}^{-1}$ , which is characteristic of free *deta*, shifts to a higher frequency ( $1604\text{ cm}^{-1}$ ) after bonding to  $\text{Cu(II)}$ .

Table 2 lists the bond lengths and bond angles for **1**. The  $\text{Cu}^{2+}$  ion is hexacoordinated by N atoms. The coordination sphere around the central atom is a distorted tetragonal bipyramid. The base of the polyhedron is formed by N(1), N(2), and N(3) atoms from the first *deta* molecule and N(5) atom from the second *deta* molecule. The apical positions are occupied by N(4) and N(6) atoms from the second *deta* molecule. The Cu–N bond lengths in the bipyramid equatorial plane range from  $2.019(1)$  to  $2.084(1)\text{ \AA}$ , while the axial Cu(1)–N(4) and Cu(1)–N(6) bonds are longer with the distances of  $2.372(1)$  and  $2.485(1)\text{ \AA}$ , respectively. The observed loosening of the Cu(1)–N(4) and Cu(1)–N(6) bonds is mainly caused by the electrostatic repulsion of the electron lone pair of nitrogen atoms from the electron pair located on the  $d_{z^2}$   $d_{z^2}$  atomic orbital (AO) of the  $\text{Cu}^{2+}$  ion, known as the Jahn-Teller effect.<sup>54</sup>

In **1**, chloride anions are hydrated by water molecules and also form hydrogen bonds with coordinated *deta* molecules. Therefore, the complex  $[\text{Cu}(\text{deta})_2]^{2+}$  cations are linked to external chloride anions through a bridging water molecule. As a result, a branched system of fairly strong hydrogen bonds  $\text{N-H}\cdots\text{H}_2\text{O}\cdots\text{Cl}$  is formed in **1** (distances N(3)–H(31N) $\cdots$ O(1) and O(1)–H(2W) $\cdots$ Cl(1) are  $2.39(2)$  and  $2.37\text{ \AA}$ , respectively) (Table 3). These hydrogen bonds provide a directional character to the ionic interaction between cation and anion. The investigated hydrogen bonds are a vivid example of the particular influence of directed ionic interaction on the formation of the crystal structure.<sup>55–57</sup>

Fig. 5 displays a two-dimensional plot of the contacts' fingerprints separated into H $\cdots$ H, H $\cdots$ Cl, and H $\cdots$ O, along with their corresponding contributions to the Hirshfeld surface. The most significant interaction is H $\cdots$ H, which accounts for 76.8% of the HS. This is due

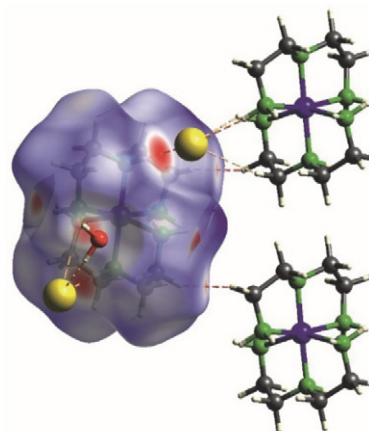


Figure 4. Hirshfeld surface for **1** mapped with  $d_{\text{norm}}$  over the range  $-0.382$  to  $1.306\text{ a.u.}$  Neighboring  $[\text{Cu}(\text{deta})_2]^{2+}$  cations associated with hydrogen bonds are also shown.

Table 2. The bond lengths and bond angles in **1**

Bond	<i>d</i> , Å	Angle	$\omega$ , °
Cu(1)–N(1)	2.084(1)	N(1)–Cu(1)–N(2)	83.73(4)
Cu(1)–N(2)	2.019(1)	N(1)–Cu(1)–N(3)	165.41(4)
Cu(1)–N(3)	2.058(1)	N(1)–Cu(1)–N(4)	90.20(4)
Cu(1)–N(4)	2.372(1)	N(1)–Cu(1)–N(5)	97.42(4)
Cu(1)–N(5)	2.041(1)	N(1)–Cu(1)–N(6)	86.20(4)
Cu(1)–N(6)	2.485(1)	N(2)–Cu(1)–N(3)	83.83(4)
		N(2)–Cu(1)–N(4)	99.94(4)
N(1)–C(1)	1.482(1)	N(2)–Cu(1)–N(5)	178.84(4)
N(2)–C(2)	1.468(1)	N(2)–Cu(1)–N(6)	101.69(4)
N(2)–C(3)	1.479(1)	N(3)–Cu(1)–N(4)	99.43(4)
N(3)–C(4)	1.480(1)	N(3)–Cu(1)–N(5)	95.03(4)
N(4)–C(5)	1.473(2)	N(3)–Cu(1)–N(6)	88.89(4)
N(5)–C(6)	1.480(1)	N(4)–Cu(1)–N(5)	80.06(4)
N(5)–C(7)	1.479(1)	N(4)–Cu(1)–N(6)	78.45(4)
N(6)–C(8)	1.471(2)	N(5)–Cu(1)–N(6)	157.57(4)
C(1)–C(2)	1.520(2)		
C(3)–C(4)	1.516(2)	N(1)–C(1)–C(2)	109.1(1)
C(5)–C(6)	1.516(2)	C(1)–C(2)–N(2)	107.0(1)
C(7)–C(8)	1.521(2)	C(2)–N(2)–C(3)	115.8(1)
		N(2)–C(3)–C(4)	107.3(1)
N–H	0.80(2)–0.89(2)	C(3)–C(4)–N(3)	108.3(1)
C–H	0.99	N(4)–C(5)–C(6)	109.8(1)
O–H	0.85	C(5)–C(6)–N(5)	109.6(1)
		C(6)–N(5)–C(7)	114.3(1)
		N(5)–C(7)–C(8)	109.8(1)
		C(7)–C(8)–N(6)	110.0(1)

Table 3. Geometry of selected hydrogen bonds in **1**

D–H...A	Symmetry code	Distances, Å			Angle, °
		D–H	H...A	D...A	D–H...A
N(1)–H(11N)...Cl(1)		0.87(2)	2.51(2)	3.362(1)	169(1)
N(1)–H(12N)...Cl(1)	$-x + 2, -y + 1, -z + 1$	0.83(2)	2.57(2)	3.396(1)	174(1)
N(2)–H(21N)...Cl(1)	$x, -y + 1/2, z + 1/2$	0.88(2)	2.43(2)	3.304(1)	169(1)
N(3)–H(31N)...O(1)		0.82(2)	2.39(2)	3.131(2)	150(1)
N(3)–H(32N)...Cl(2)	$-x + 1, -y + 1, -z + 1$	0.84(2)	2.61(2)	3.375(1)	153(1)
N(5)–H(51N)...Cl(2)		0.80(2)	2.52(2)	3.308(1)	169(1)
N(6)–H(61N)...Cl(1)		0.89(2)	2.58(2)	3.402(1)	155(1)
N(6)–H(62N)...Cl(2)	$-x + 1, -y + 1, -z + 1$	0.83(2)	2.64(2)	3.385(1)	151(1)
O(1)–H(1W)...Cl(2)		0.85	2.41	3.195	153
O(1)–H(2W)...Cl(2)	$-x + 1, y + 1/2, -z + 1/2$	0.85	2.37	3.196	166

to the large number of H atoms in the discrete cation  $[\text{Cu}(\text{deta})_2]^{2+}$ , resulting in widely scattered points of high density. The spike with a tip at  $d_e + d_i \approx 2.04$  Å (Fig. 5a) is due to short interatomic contacts between methylene groups. The next significant interaction is H...Cl, which contributes 19.1% to the HS (Fig. 5b). The distribution of points in this interaction is asymmetric and is caused by the N–H...Cl hydrogen bonds (Table 3). It is considered a sharp spike with a tip at  $d_e + d_i \approx 2.24$  Å. The interaction H...O contributes 4.1% to the HS in the form of a compact distribution of points (Fig. 5c). It arises from the N–H...O

hydrogen bonds (Table 3) and is considered a spike with a tip at  $d_e + d_i \approx 2.25$  Å.

### 3. 2. Electronic Structure of $[\text{Cu}(\text{deta})_2]\text{Cl}_2 \cdot \text{H}_2\text{O}$

The interaction between Cu(II) and *deta* alters the electronic characteristics of the coordinated *deta* molecule compared to the uncoordinated molecule. DFT calculations indicate that the electronic density of the ligand molecule's nitrogen atoms in the coordination core of **1** shift

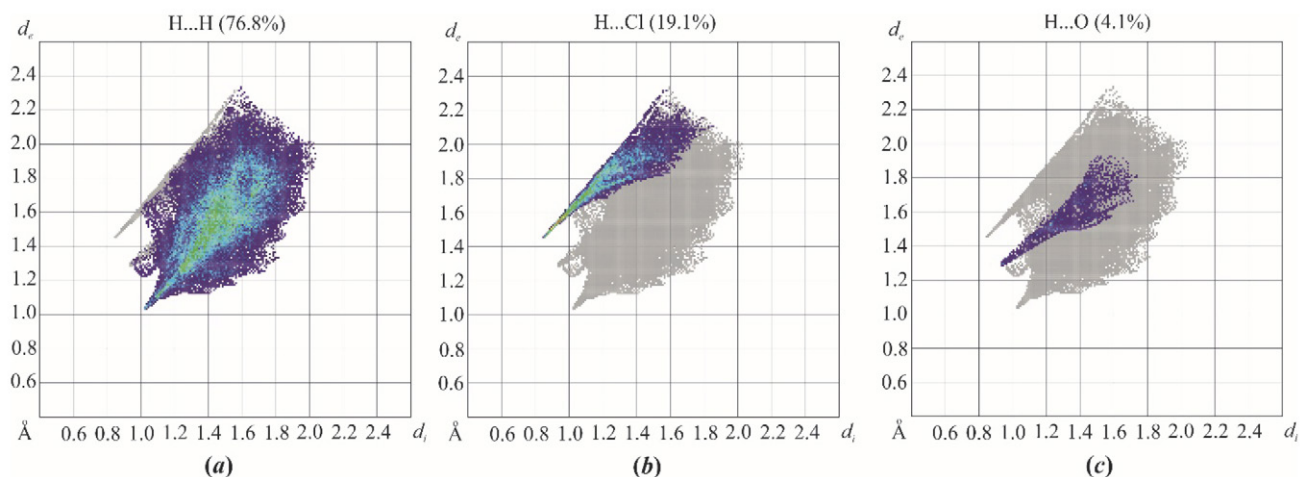


Figure 5. Fingerprint plots resolved into H...H (a), H...Cl (b) and H...O (c) contacts.

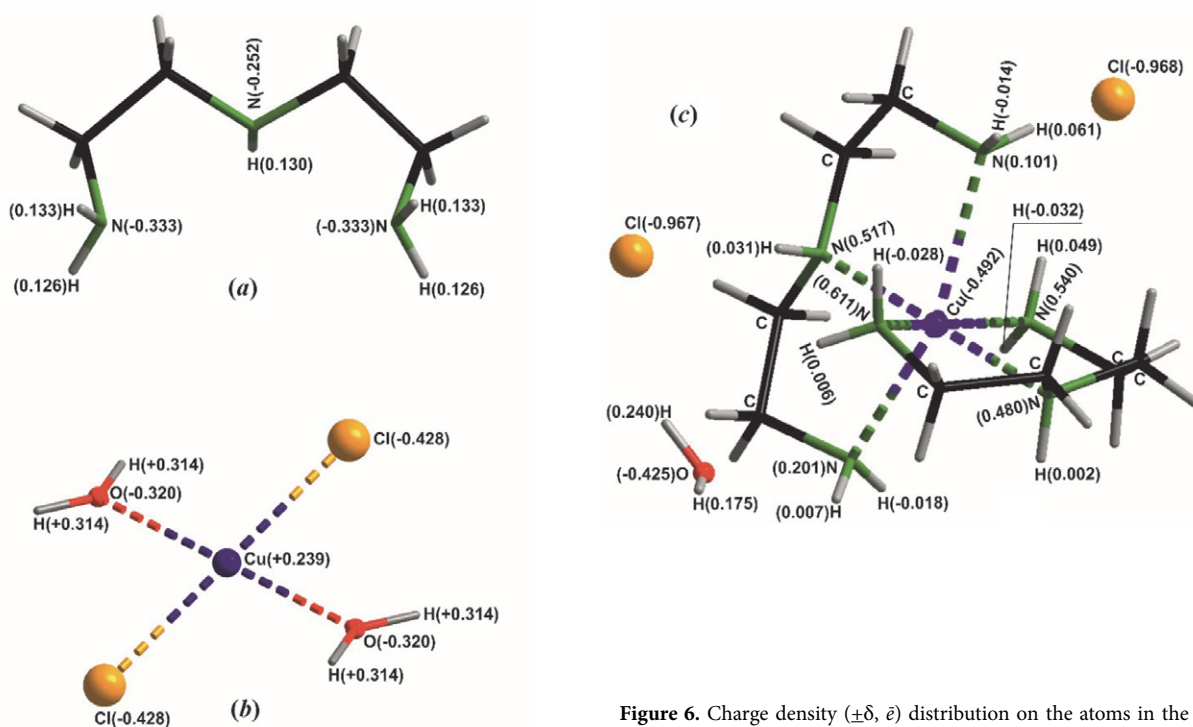
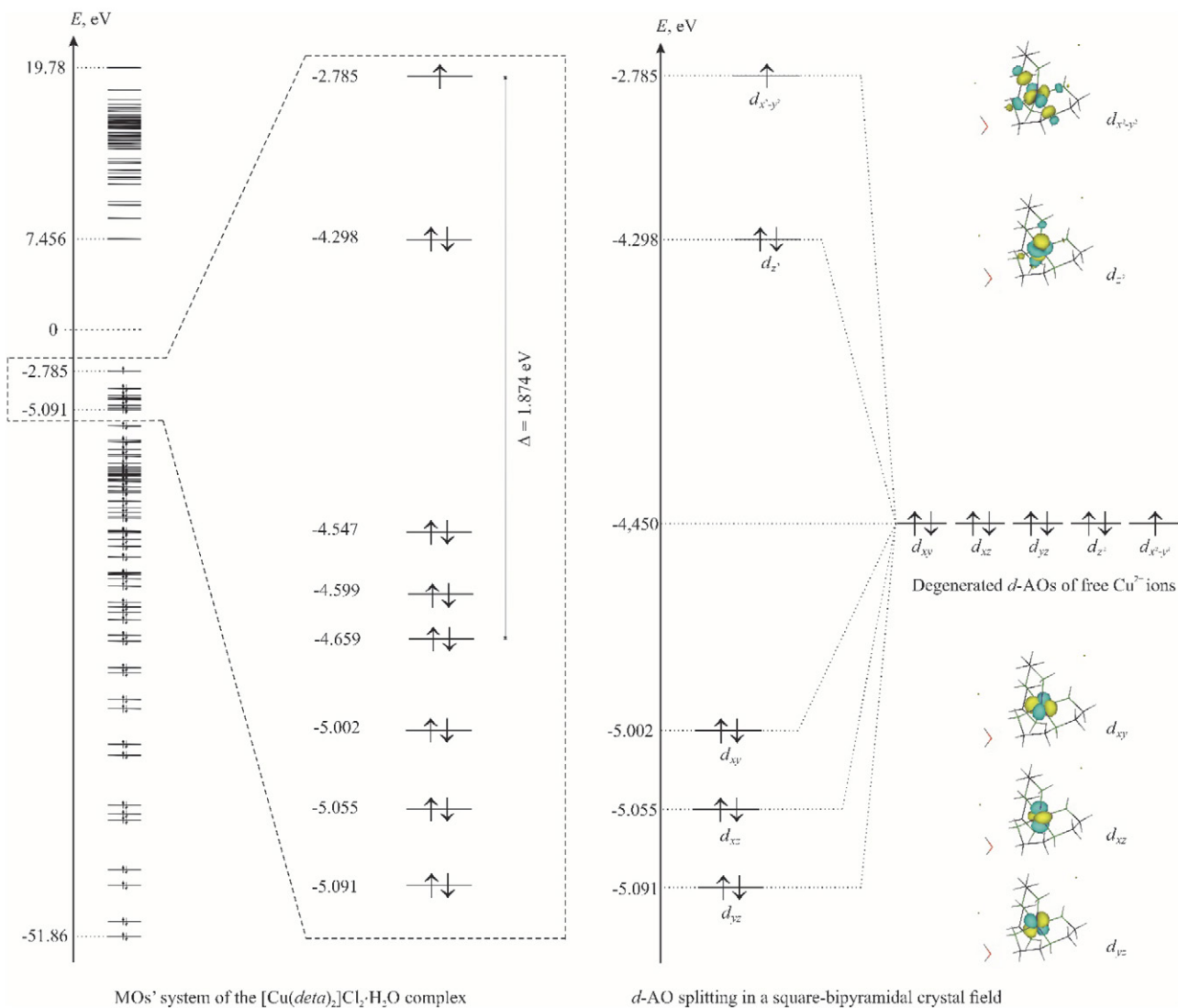


Figure 6. Charge density ( $\pm\delta$ ,  $e$ ) distribution on the atoms in the *deta* (a),  $[\text{Cu}(\text{H}_2\text{O})_2\text{Cl}_2]$  (b), and  $[\text{Cu}(\text{deta})_2]\text{Cl}_2 \cdot \text{H}_2\text{O}$  (c).

towards the Cu(II) atom. So, the value of charge density ( $d$ ) on nitrogen atoms of uncoordinated *deta* molecule are  $-0.333 \bar{e}$  (for  $-\text{NH}_2$  groups) and  $-0.252 \bar{e}$  (for  $-\text{NH}$ -group), and the  $d$  value on Cu atom in  $[\text{Cu}(\text{H}_2\text{O})_2\text{Cl}_2]$  unit fragment of the copper(II) chloride equals to  $+0.239 \bar{e}$  (Fig. 6, a and b). However, chelation reduces the electron density on the nitrogen atoms of the coordinated *deta* molecule in the coordination core  $[\text{Cu}(\text{deta})_2]\text{Cl}_2 \cdot \text{H}_2\text{O}$ . The  $d$  values for axially bonded N atoms range from  $+0.101$  to  $+0.201 \bar{e}$ , while for N atoms bonded at the equatorial plane of the bipyramid, the  $d$  values range from  $+0.480$  to  $+0.611 \bar{e}$ . In contrast, the chelated Cu(II) atom accumulates an electron density of  $-0.492 \bar{e}$  (Fig. 6, c).

Due to chelation, the lone electron pairs of N-atoms of the *deta* overlap more efficiently with four of the six unoccupied  $d_{x^2-y^2} d_{z^2}$ -hybridized AOs of the central  $\text{Cu}^{2+}$  ion directed to the vertices of the square base. The other two hybridized atomic orbitals of the  $\text{Cu}^{2+}$  ion are also overlapped with the apical N atoms, but less effectively. Thus, the initially octahedral environment of the metal atom is strongly deformed and takes on the shape of an elongated tetragonal bipyramid. The square-bipyramidal field of ligands, along with the chelating effect, eliminates the degeneration of the  $3d$ -AO of the  $\text{Cu}^{2+}$  ion in **1**. Fig. 7 shows the MO diagram for  $[\text{Cu}(\text{deta})_2]\text{Cl}_2 \cdot \text{H}_2\text{O}$  and the  $3d$ -AO splitting of the  $\text{Cu}^{2+}$  ion in spherical and square-bipyramidal crystal fields.



**Figure 7.** MO diagram for [Cu(deta)<sub>2</sub>]Cl<sub>2</sub>·H<sub>2</sub>O (left) and 3d-AO splitting of Cu<sup>2+</sup> ion in spherical and square-bipyramidal crystal fields (right).

Based on the crystal field theory,<sup>58</sup> the degenerate 3d atomic orbitals (AO) of the complexing agent in the octahedral ligand environment split into two sets of AOs with different energies. The set consisting of  $d_{yz}$ ,  $d_{xz}$ , and  $d_{xy}$ -AOs has the lowest energy, while the  $d_{z^2}$ - and  $d_{x^2-y^2}$ -AOs have the highest energy. The coordination environment of the Cu<sup>2+</sup> ion is deformed to a square-bipyramidal one due to the Jahn-Teller effect and the chelating effect. The arrangement of the split d-AOs in the square-bipyramidal crystal field of ligands results in a slightly different sequence of the complexing agent's splitting parameters. The energy levels follow this order (in ascending order of AO energy):  $d_{yz} < d_{xz} < d_{xy}$  and  $d_{z^2} < d_{x^2-y^2}$  (refer to Fig. 7). The energy difference between the  $d_{yz}$ -AO, which has the lowest energy, and the  $d_{x^2-y^2}$ -AO, which has the highest energy, is 2.306 eV. Between these energy levels is a portion of the molecular orbitals (MO) of the complex, resulting in the emergence of a distinct gap ( $D = 1.874$  eV) between

the energy levels of the corresponding MO (-4.659 eV) occupied by a pair of electrons and  $d_{x^2-y^2}$ -AO (-2.785 eV) with an unpaired electron. The energy gap corresponds precisely to the wavelength of visible light ( $\lambda = 661.37$  nm). This energy is adequate to transfer one electron from a lower energy level to a higher one, resulting in an excited state. The energy difference between the ground and excited states equals the energy of the absorbed photon with the wavelength of 661.37 nm. This is why crystal **1** appears dark blue.

### 3. 3. Flame Retardant Properties of [Cu(deta)<sub>2</sub>]Cl<sub>2</sub>·H<sub>2</sub>O

The thermal behavior of chelate complex **1**, used as a flame retardant-hardener for epoxy resins, largely depends on the efficiency of bonding of combustible *deta* to non-combustible copper(II) chloride. The thermal properties

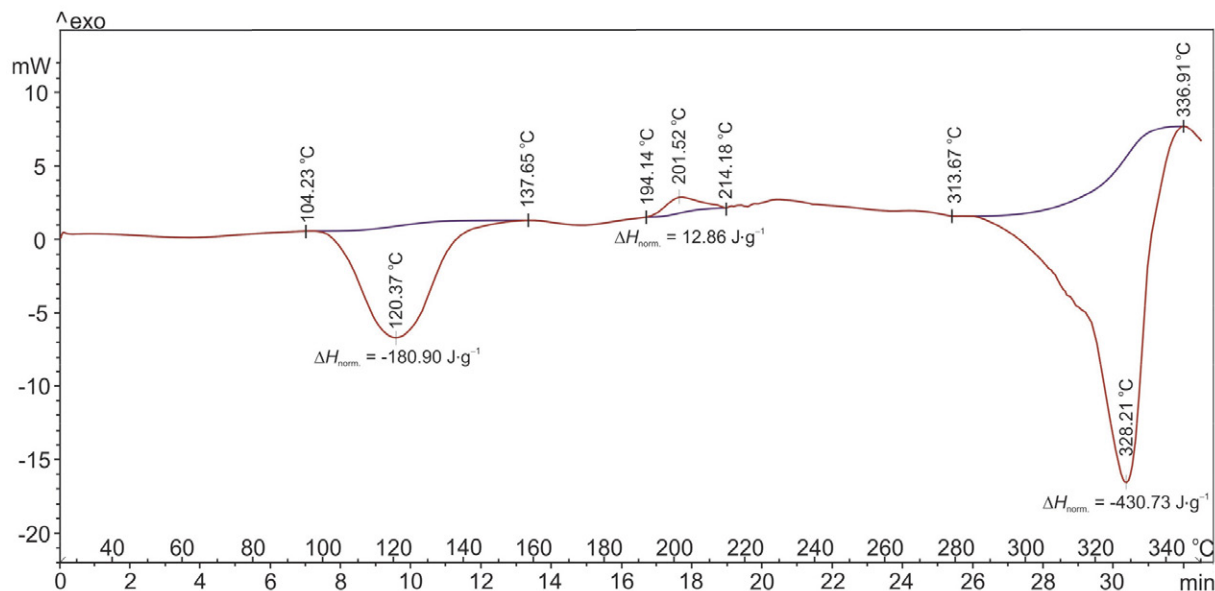


Figure 8. DSC curve of **1**

of **1** were analyzed through differential scanning calorimetry, and the DSC results are presented in Fig. 8.

The DSC curve shows that the thermal behavior of **1** can be divided into three temperature regions. The first region, spanning from 104.23 to 137.65 °C, absorbs 64.9 kJ·mol<sup>-1</sup> of heat. At 120.37 °C, an endothermic minimum appears, indicating the release of crystallization water from the crystals of **1**.

The second stage of thermal decomposition of **1** occurs between 194.14 and 214.18 °C, with a slight exothermic peak at 201.52 °C, releasing 4.6 kJ mol<sup>-1</sup> of heat. In this temperature range, crystals **1** melt and decompose simultaneously. At the same time, it is the amine component that undergoes partial thermal degradation, including dehydrogenation of the metal-coordinated *deta* with simultaneous hydrogen release.

The third and final stage of thermal decomposition absorbs the largest amount of thermal energy, specifically 154.5 kJ mol<sup>-1</sup>. This endothermic process occurs within a temperature range of 313.67 to 336.92 °C, with an endothermic minimum at 328.31 °C. During this process, Cu–N coordination bonds are broken, resulting in the complete destruction of the complex.

Finally, it is important to consider the effect of the interaction between *deta* and CuCl<sub>2</sub> on the combustibility of *deta*. For instance, while the ignition temperature of free *deta* is 97 °C, *deta* bound in the complex does not ignite at all, even if the temperature reaches 450 °C. In other words, the combustible *deta* (epoxy hardener) becomes a virtually non-combustible substance after bonding to copper(II) chloride (flame retardant). This phenomenon is attributed to the coordination bonds between *deta* and CuCl<sub>2</sub>, known as Cu(II) ← N bonds. Breaking these bonds requires

338.34 kJ·mol<sup>-1</sup> of thermal energy, which firmly holds the *deta* molecules in the complex and makes them extremely resistant to thermo-oxidative degradation. The flame retardant effect of inorganic copper(II) salts on the combustion of nitrogen-containing hydrocarbons is due to complexation processes.

## 4. Conclusions

The chelated complex [Cu(*deta*)<sub>2</sub>]Cl<sub>2</sub>·H<sub>2</sub>O (**1**) was synthesized by reacting CuCl<sub>2</sub>·2H<sub>2</sub>O with *deta*. Complex **1** is composed of discrete complex cations – [Cu(*deta*)<sub>2</sub>]<sup>2+</sup>, where *deta* molecules act as chelating agents, and hydrated anions [Cl··H<sub>2</sub>O··Cl]<sup>2-</sup>. The Cu<sup>2+</sup> ion in [Cu(*deta*)<sub>2</sub>]<sup>2+</sup> is hexacoordinated by the N-atoms of two *deta* molecules, determining the geometry of the coordination polyhedron of Cu(II), which has the shape of a distorted tetragonal bipyramid. The crystal framework of the complex is stabilized by hydrogen bonds N–H··O, N–H··Cl and O–H··Cl. An analysis of the electronic structure of **1** using quantum chemistry calculations revealed that the square-bipyramidal crystal field of ligands and the chelating effect work together to split the degenerate 3d-AOs of the Cu<sup>2+</sup> ion into two sets of energy levels. One set has lower energy ( $d_{yz} < d_{xz} < d_{xy}$ ), and the other has higher energy ( $d_{z^2} < d_{x^2-y^2}$ ). The chelating effect has an impact on the thermal behavior of solid complex **1**. Therefore, DSC studies and flammability tests have demonstrated that the decomposition of crystalline complex **1** is completed at a temperature of 328 °C, while the ignition of *deta* bonded in the complex does not occur at all. This indicates that crystals **1** can be utilized as a flame retardant-hardener for epoxy resins.

## Acknowledgment

We are grateful to Dr. Błażej Dziuk (University of Opole) for help in X-ray diffraction measurements.

## Declaration of Competing Interest

No potential conflict of interest was reported by the authors.

## Supplementary material

CCDC reference number 2348476 contains the supplementary crystallographic data for **1**. These data can be obtained free of charge via <http://www.ccdc.cam.ac.uk/conts/retrieving.html> or from the Cambridge Crystallographic Data Center, 12 Union Road, Cambridge CB2 1EZ, UK; Fax: +441223336033; E-mail: [deposit@ccdc.cam.ac.uk](mailto:deposit@ccdc.cam.ac.uk). Supplementary data associated with this article can be found in the online version.

## 6. References

- B. M. Mykhalichko, O. N. Temkin, M. G. Mys'kiv, *Russ. Chem. Rev.* **2000**, *69*, 957–984. DOI:10.1070/RC2000v069n11ABEH000609
- O. N. Temkin, P. P. Pozdeev: Homogeneous Catalysis with Metal Complexes. Kinetics Aspects and Mechanisms, John Wiley & Sons, New York, **2012**. DOI:10.1002/9781119966227
- H. V. R. Dias, H.-L. Lu, H.-J. Kim, S. A. Polach, T. K. Goh, R. G. Browning, C. J. Lovely, *Organometallics* **2002**, *21*, 1466–1473. DOI:10.1021/om010886v
- B. F. Straub, F. Eisenträger, P. Hofmann, *Chem. Commun.* **1999**, *24*, 2507–2508. DOI:10.1039/A907928I
- Z. Li, R. W. Quan, E. N. Jacobsen, *J. Am. Chem. Soc.* **1995**, *117*, 5889–5890. DOI:10.1021/ja00126a044
- P. Brandt, M. J. Södergren, P. G. Andersson, P. Norrby, *J. Am. Chem. Soc.* **2000**, *122*, 8013–8020. DOI:10.1021/ja993246g
- K. M. Gillespie, C. J. Sanders, P. O'Shaughnessy, I. Westmoreland, C. P. Thickitt, P. Scott, *J. Org. Chem.* **2002**, *67*, 3450–3458. DOI:10.1021/jo025515i
- F. I. Rodríguez, J. J. Esch, A. E. Hall, B. M. Binder, G. E. Schaller, A. B. Blecker, *Science*. **1999**, *283*, 996–998. DOI:10.1126/science.283.5404.996
- F. B. Abeles, P. V. Morgan, M. E. Selveit: Ethylene in Plant Biology, Academic Press, San Diego, **1992**.
- J. Zhang, R.-G. Xiong, X.-T. Chen, Z. Xue, S.-M. Peng, X.-Z. You, *Organometallics*. **2002**, *21*, 235–238. DOI:10.1021/om010665p
- J. Zhang, R.-G. Xiong, J.-L. Zuo, X.-Z. You, *Chem. Commun.* **2000**, *16*, 1495–1496. DOI:10.1039/b004001k
- H. Lavrenyuk, V. Kochubei, O. Mykhalichko, B. Mykhalichko, *Fire Saf. J.* **2016**, *80*, 30–37. DOI:10.1016/j.firesaf.2016.01.001
- H. Lavrenyuk, V. Kochubei, B. Mykhalichko, O. Mykhalichko, *Fire Mater.* **2018**, *42*, 266–277. DOI:10.1002/fam.2489
- H. Lavrenyuk, B. Mykhalichko, P. Garanyuk, O. Mykhalichko, *Fire Mater.* **2020**, *44*, 825–834. DOI:10.1002/fam.2879
- H. Lavrenyuk, V. Kochubei, B. Mykhalichko, O. Mykhalichko, *Polym. Bull.* **2022**, *79*, 157–178. DOI:10.1007/s00289-020-03499-4
- H. Lavrenyuk, V. Kochubei, B. Mykhalichko, O. Mykhalichko, *J. Therm. Anal. Calorim.* **2022**, *147*, 2197–2207. DOI:10.1007/s10973-021-10622-8
- G.-X. He, X.-Y. Guo, L.-W. Xue, *Acta Chim. Slov.* **2023**, *70*, 148–154. DOI:10.17344/acsi.2022.7815
- M. G. Mys'kiv, B. M. Mykhalichko, *J. Struct. Chem.* **1994**, *35*, 677–687. DOI:10.1007/BF02578338
- G. V. Noshchenko, B. M. Mykhalichko, V. V. Kinzhybalov, *J. Coord. Chem.* **2021**, *74*, 955–968. DOI:10.1080/00958972.2020.1869727
- I. Hamerton, B. Howlin, P. Jepson, *Coord. Chem. Rev.* **2002**, *224*, 67–85. DOI:10.1016/S0010-8545(01)00393-9
- H. Lavrenyuk, B. Mykhalichko, *Voprosy Khimii i Khimicheskoi Tekhnologii.* **2018**, *6*, 42–48. DOI:10.32434/0321-4095-2018-121-6-42-48
- H. Lavrenyuk, B. Mykhalichko, V.-P. Parhomenko, *Voprosy Khimii i Khimicheskoi Tekhnologii.* **2018**, *3*, 31–36.
- H. Lavrenyuk, I. Hamerton, B. Mykhalichko, *React. Funct. Polym.* **2018**, *129*, 95–102. DOI:10.1016/j.reactfunctpolym.2017.10.013
- H. Lavrenyuk, B. Mykhalichko, V.-P. Parhomenko, *Int. J. Technol.* **2019**, *10*, 290–299. DOI:10.14716/ijtech.v10i2.66
- B. Mykhalichko, H. Lavrenyuk, *Period. Polytech. Chem. Eng.* **2022**, *66*, 304–312. DOI:10.3311/PPch.19050
- B. Mykhalichko, V. Kochubei, H. Lavrenyuk, *Fire Mater.* **2022**, *46*, 587–594. DOI:10.1002/fam.3008
- M. Julve, M. Verdager, J. Fans, F. Tinti, J. Moratal, A. Monge, E. Gutierrez-Puebla, *Inorg. Chem.* **1987**, *26*, 3520–3527. DOI:10.1021/ic00268a021
- P. Xu, C. Chen, Y. Xu, C. Cheng, J. Chen, W. Tang, *Acta Cryst.* **1991**, *C47*, 72–75. DOI:10.1107/S0108270190007223
- C.-C. Su, C.-Y. Wu, *J. Coord. Chem.* **1994**, *33*, 1–14. DOI:10.1080/00958979408024257
- P. S. Subramanian, E. Suresh, R. S. Shukla, *Inorg. Chim. Acta.* **2005**, *358*, 2651–2660. DOI:10.1016/j.ica.2005.03.007
- R. N. Patel, N. Singh, K. K. Shukla, J. Niclós-Gutiérrez, A. Castineiras, V. G. Vaidyanathan, B. U. Nair, *Spectrochim. Acta A.* **2005**, *62*, 261–268. DOI:10.1016/j.saa.2004.12.034
- F. S. Stephens, *J. Chem. Soc. A.* **1969**, 883–890. DOI:10.1039/j19690000883
- M. K. Urriaga, M. I. Arriortua, R. Cortés, T. Rojo, *Acta Crystallogr.* **1996**, *C52*, 3007–3009. DOI:10.1107/S010827019600978X
- M. J. Begley, P. Hubberstey, J. Stroud, *Polyhedron.* **1997**, *16*, 805–813. DOI:10.1016/S0277-5387(96)00338-5
- H.-L. Zhu, H.-L. Liu, Y.-H. Li, K.-B. Yu, Z. *Kristallogr. NCS.* **2003**, *218*, 41–42. DOI:10.1524/ncrs.2003.218.1.41
- H. Lavrenyuk, O. Mykhalichko, B. Zarychta, V. Olijnyk, B. Mykhalichko, *J. Mol. Struct.* **2015**, *1095*, 34–41.

- DOI:10.1016/j.molstruc.2015.03.039
37. H. Lavrenyuk, O. Mykhalichko, B. Zarychta, V. Olijnyk, B. Mykhalichko, *J. Coord. Chem.* **2016**, *69*, 2666–2676.  
DOI:10.1080/00958972.2016.1212340
38. H. Lavrenyuk, B. Mykhalichko, B. Dziuk, V. Olijnyk, O. Mykhalichko, *Arab. J. Chem.* **2020**, *13*, 3060–3069.  
DOI:10.1016/j.arabjc.2018.08.014
39. B. Mykhalichko, H. Lavrenyuk, O. Mykhalichko, *Turk. J. Chem.* **2021**, *45*, 1865–1872. DOI:10.3906/kim-2106-9
40. A. G. Brook, *Am. Miner.* **1950**, *35*, 447.
41. Oxford Diffraction. *CrysAlis CCD, Data collection GUI for CCD and CrysAlis RED, CCD data reduction GUI (Version 1.171)*, Oxford Diffraction, Wroclaw (2002).
42. G. M. Sheldrick, *Acta Crystallogr. Sect. A, Found. Adv.* **2015**, *71*, 3–8. DOI:10.1107/S2053273314026370
43. G. M. Sheldrick, *Acta Crystallogr. Sect. C, Struct. Chem.* **2015**, *71*, 3–8. DOI:10.1107/S2053229614024218
44. O. V. Dolomanov, L. J. Bourhis, R. J. Gildea, J. A. K. Howard, H. Puschmann, *J. Appl. Crystallogr.* **2009**, *42*, 339–341.  
DOI:10.1107/S0021889808042726
45. K. Brandenburg, H. Putz. *DIAMOND*, Crystal Impact GbR, Bonn, Germany (2012).
46. ASTM D1929-20 Standard Test Method for Determining Ignition Temperature of Plastics, ASTM International, West Conshohocken, PA, USA (2020). DOI:10.1520/D1929-20
47. HyperChem: Molecular Modeling System, Hypercube, Inc., Release 8.0.6, Florida (2010).
48. S. Brownstein, N. F. Han, E. Gabe, Y. LePage, *Z. Kristallogr. Cryst. Mater.* **1989**, *189*, 13–15.  
DOI:10.1524/zkri.1989.189.14.ack
49. P. R. Spackman, M. J. Turner, J. J. McKinnon, S. K. Wolff, D. J. Grimwood, D. Jayatilaka, M. A. Spackman, *J. Appl. Crystallogr.* **2021**, *54*, 1006–1011. DOI:10.1107/S1600576721002910
50. F. S. Stephens, *J. Chem. Soc. A: Inorg. Phys. Theor.* **1969**, 2233–2240. DOI:10.1039/j19690002233
51. R. C. Hynes, C. J. Willis, J. J. Vittal, *Acta Crystallogr. Sect. C, Cryst. Struct. Commun.* **1996**, *52*, 1879–1881.  
DOI:10.1107/S0108270196005835
52. B. Liu, F.-J. Huo, X.-M. Jiang, B.-S. Yang, *Acta Crystallogr. Sect. E, Struct. Reports Online.* **2005**, *61*, m598–m600.  
DOI:10.1107/S160053680500560X
53. H.-J. Li, L.-M. Sun, Z.-H. Liu, *Acta Crystallogr. Sect. E, Struct. Reports Online.* **2006**, *62*, m2522–m2523.  
DOI:10.1107/S1600536806035896
54. K. Tanaka, M. Konishi, F. Marumo, *Acta Cryst.* **1979**, *B35*, 1303–1308. DOI:10.1107/S0567740879006312
55. G. R. Desiraju, *J. Chem. Soc., Dalton Trans.* **2000**, *21*, 3745–3751. DOI:10.1039/b003285i
56. G. R. Desiraju, *Acc. Chem. Res.* **2002**, *35*, 565–573.  
DOI:10.1021/ar010054t
57. A. Fedorchuk, E. Goreschnik, Y. Slyvka, M. Mys'kiv, *Acta Chim. Slov.* **2020**, *67*, 1148–1154.  
DOI:10.17344/acsi.2020.6045
58. J. H. Van Vleck, *Phys. Rev.* **1932**, *41*, 208–215.  
DOI:10.1103/PhysRev.41.208

## Povzetek

Kelatni kompleks bakrovega(II) klorida z dietilenetriaminom (*deta*),  $[\text{Cu}(\textit{deta})_2]\text{Cl}_2 \cdot \text{H}_2\text{O}$  (**1**), smo sintetizirani z neposredno interakcijo trdnega bakrovega(II) klorida dihidrata z *deta*. S pomočjo rentgenske strukturne analize, infrardeče (IR) spektroskopije in diferenčne dinamične kalorimetrije (DSC) smo okarakterizirali kelatni kompleks **1** ter ga proučevali kot zaviralca gorenja epoksidnih smol. Kristali **1** so sestavljeni iz kationov  $[\text{Cu}(\textit{deta})_2]^{2+}$ , anionov  $\text{Cl}^-$  in nekoordiniranih molekul vode. Vsak atom Cu(II) je kelatiran z dvema tridentatnima molekulama *deta*, ki se neekvivalentno vežeta na osrednji atom Cu(II). Posledica tega je popačena tetragonalno bipiramidna razporeditev okoli Cu(II). Kristalno pakiranje strukturnih enot v **1** določajo prevladujoča interakcija med kationom in anionom ter močne vodikove vezi, kot so  $\text{N}-\text{H}\cdots\text{Cl}$ ,  $\text{N}-\text{H}\cdots\text{O}$ , and  $\text{O}-\text{H}\cdots\text{Cl}$ . S teorijo gostotnostnega funkcionala (DFT) smo določili elektronsko strukturo **1** ob uporabi metode B3LYP in baznega seta 6-31G\*. Opazen je razcep *d*-orbital  $\text{Cu}^{2+}$  zaradi tetragonalne bipiramidalne razporeditve ligandov in kelacije, kar povzroči temno modro barvo kristalov **1**. Barva se ujema z izračunano vrednostjo valovne dolžine vidne svetlobe ( $\lambda = 661,37$  nm), ki je povezana z energijo fotonov, ki jih kompleks absorbira ( $\Delta = 1,874$  eV).



Except when otherwise noted, articles in this journal are published under the terms and conditions of the Creative Commons Attribution 4.0 International License